We are IntechOpen, the world's leading publisher of Open Access books Built by scientists, for scientists

6,900
Open access books available

185,000
International authors and editors

200M
Downloads

Our authors are among the

154
Countries delivered to

TOP 1%
most cited scientists

12.2%
Contributors from top 500 universities



WEB OF SCIENCE™

Selection of our books indexed in the Book Citation Index in Web of Science™ Core Collection (BKCI)

Interested in publishing with us?
Contact book.department@intechopen.com

Numbers displayed above are based on latest data collected.
For more information visit www.intechopen.com



9

Acceleration-based 3D Flight Control for UAVs: Strategy and Longitudinal Design

Iain K. Peddle and Thomas Jones
Stellenbosch University
South Africa

1. Introduction

The design of autopilots for conventional flight of UAVs is a mature field of research. Most of the published design strategies involve linearization about a trim flight condition and the use of basic steady state kinematic relationships to simplify control law design (Blakelock, 1991);(Bryson, 1994). To ensure stability this class of controllers typically imposes significant limitations on the aircraft's allowable attitude, velocity and altitude deviations. Although acceptable for many applications, these limitations do not allow the full potential of most UAVs to be harnessed. For more demanding UAV applications, it is thus desirable to develop control laws capable of guiding aircraft though the full 3D flight envelope. Such an autopilot will be referred to as a manoeuvre autopilot in this chapter.

A number of manoeuvre autopilot design methods exist. Gain scheduling (Leith &. Leithead, 1999) is commonly employed to extend aircraft velocity and altitude flight envelopes (Blakelock, 1991), but does not tend to provide an elegant or effective solution for full 3D manoeuvre control. Dynamic inversion has recently become a popular design strategy for manoeuvre flight control of UAVs and manned aircraft (Bugajski & Enns, 1992); (Lane & Stengel, 1998);(Reiner et al., 1996);(Snell et al., 1992) but suffers from two major drawbacks. The first is controller robustness, a concern explicitly addressed in (Buffington et al., 1993) and (Reiner et al., 1996), and arises due to the open loop nature of the inversion and the inherent uncertainty of aircraft dynamics. The second drawback arises from the slightly Non Minimum Phase (NMP) nature of most aircraft dynamics, which after direct application of dynamic inversion control, results in not only an impractical controller with large counterintuitive control signals (Hauser et al., 1992) (Reiner et al., 1996), but also in undesired internal dynamics whose stability must be investigated explicitly (Slotine & Li, 1991). Although techniques to address the latter drawback have been developed (Al-Hiddabi & McClamroch, 2002);(Hauser et al., 1992), dynamic inversion is not expected to provide a very practical solution to the 3D flight control problem and should ideally only be used in the presence of relatively certain minimum phase dynamics.

Receding Horizon Predictive Control (RHPC) has also been applied to the manoeuvre flight control problem (Bhattacharya et al., 2002);(Miller & Pachter, 1997);(Pachter et al., 1998), and similarly to missile control (Kim et al., 1997). Although this strategy is conceptually very promising the associated computational burden often makes it a practically infeasible solution for UAVs, particularly for lower cost UAVs with limited processing power.

The manoeuvre autopilot solution presented in this chapter moves away from the more mainstream methods described above and instead returns to the concept of acceleration control which has been commonly used in missile applications, and to a limited extent in aircraft applications, for a number of decades (see (Blakelock, 1991) for a review of the major results). However, whereas acceleration control has traditionally been used within the framework of linearised flight control (the aircraft or missile dynamics are linearised, typically about a straight and level flight condition), the algorithms and mathematics presented in this chapter extend the fundamental acceleration controller to operate equally effectively over the entire 3D flight envelope. The result of this extension is that the aircraft then reduces to a point mass with a steerable acceleration vector from a 3D guidance perspective. This abstraction which is now valid over the entire flight envelope is the key to significantly reducing the complexity involved in solving the manoeuvre flight control problem.

The chapter thus begins by presenting the fundamental ideas behind the design of gross attitude independent specific acceleration controllers. It then highlights how these inner loop controllers simplify the design of a manoeuvre autopilot and motivates that they lead to an elegant, effective and robust solution to the problem. Next, the chapter presents the detailed design and associated analysis of the acceleration controllers for the case where the aircraft is constrained to the vertical plane. A number of interesting and useful novel results regarding aircraft dynamics arise from the aforementioned analysis. The 2D flight envelope illustrates the feasibility of the control strategy and provides a foundation for development to the full 3D case.

2. Autopilot design strategy for 3D manoeuvre flight

For most UAV autopilot design purposes, an aircraft is well modelled as a six degree of freedom rigid body with specific and gravitational forces and their corresponding moments acting on it. The specific forces typically include aerodynamic and propulsion forces and arise due to the form and motion of the aircraft itself. On the other hand the gravitational force is universally applied to all bodies in proportion to their mass, assuming an equipotential gravitational field. The sum of the specific and gravitational forces determines the aircraft's total acceleration. It is desirable to be able to control the aircraft's acceleration as this would leave only simple outer control loops to regulate further kinematic states.

Of the total force vector, only the specific force component is controllable (via the aerodynamic and propulsion actuators), with the gravitational force component acting as a well modelled bias on the system. Thus, with a predictable gravitational force component, control of the total force vector can be achieved through control of the specific force vector. Modelling the specific force vector as a function of the aircraft states and control inputs is an involved process that introduces almost all of the uncertainty into the total aircraft model. Thus, to ensure robust control of the specific force vector a pure feedback control solution is desirable. Regulation techniques such as dynamic inversion are thus avoided due to the open loop nature of the inversion and the uncertainty associated with the specific force model.

Considering the specific force vector in more detail, the following important observation is made from an autopilot design simplification point of view. Unlike the gravitational force vector which remains inertially aligned, the components that make up the specific force vector tend to remain aircraft aligned. This alignment occurs because the specific forces arise

as a result of the form and motion of the aircraft itself. For example, the aircraft's thrust vector acts along the same aircraft fixed action line at all times while the lift vector tends to remain close to perpendicular to the wing depending on the specific angle of attack. The observation is thus that the coordinates of the specific force vector in a body fixed axis system are independent of the gross attitude of the aircraft. This observation is important because it suggests that if gross attitude independent measurements of the specific force vector's body axes coordinates were available, then a feedback based control system could be designed to regulate the specific force vector independently of the aircraft's gross attitude. Of course, appropriately mounted accelerometers provide just this measurement, normalized to the aircraft's mass, thus practically enabling the control strategy through specific acceleration instead.

With gross attitude independent specific acceleration controllers in place, the remainder of a full 3D flight autopilot design is greatly simplified. From a guidance perspective the aircraft reduces to a point mass with a fully steerable acceleration vector. Due to the acceleration interface, the guidance dynamics will be purely kinematic and the only uncertainty present will be that associated with gravitational acceleration. The highly certain nature of the guidance dynamics thus allows among others, techniques such as dynamic inversion and RHPC to be effectively implemented at a guidance level. In addition to the associated autopilot simplifications, acceleration based control also provides for a robust autopilot solution. All aircraft specific uncertainty remains encapsulated behind a wall of high bandwidth specific acceleration controllers. Furthermore, high bandwidth specific acceleration controllers would be capable of providing fast disturbance rejection at an acceleration level, allowing action to be taken before the disturbances manifest themselves into position, velocity and attitude errors.

With the novel control strategy and its associated benefits conceptually introduced the remainder of this chapter focuses on the detailed development of the inner loop specific acceleration controllers for the case where the aircraft's motion is constrained to the 2D vertical plane. No attention will be given to outer guidance level controllers in the knowledge that control at this level is simplified enormously by the inner loop controllers. The detailed design of the remaining specific acceleration controllers to complete the set of inner loop controllers for full 3D flight are presented in (Peddle, 2008).

3. Modelling

To take advantage of the potential of regulating the specific acceleration independently of the aircraft's gross attitude requires writing the equations of motion in a form that provides an appropriate mathematical hold on the problem. Conceptually, the motion of the aircraft needs to be split into the motion of a reference frame relative to inertial space (to capture the gross attitude and position of the aircraft) and the superimposed rotational motion of the aircraft relative to the reference frame. With this mathematical split, it is expected that the specific acceleration coordinates in the reference and body frames will remain independent of the attitude of the reference frame. An obvious and appropriate choice for the reference frame is the commonly used wind axis system (axial unit vector coincides with the velocity vector). Making use of this axis system, the equations of motion are presented in the desired form below. The dynamics are split into the point mass kinematics (motion of the wind axis system through space),

$$\dot{\Theta}_W = -\left(C_W + g\cos\Theta_W\right)/\bar{V} \tag{1}$$

$$\dot{\bar{V}} = A_W - g\sin\Theta_W \tag{2}$$

$$\dot{P}_N = \bar{V}\cos\Theta_W \tag{3}$$

$$\dot{P}_D = -\bar{V}\sin\Theta_W \tag{4}$$

and the rigid body rotational dynamics (attitude of the body axis system relative to the wind axis system),

$$\dot{Q} = M/I_{yy} \tag{5}$$

$$\dot{\alpha} = Q + \left(C_W + g\cos\Theta_W\right)/\bar{V} \tag{6}$$

with, Θ_W the flight path angle, $\bar{V}$ the velocity magnitude, P_N and P_D the north and down positions, g the gravitational acceleration, Q the pitch rate, M the pitching moment, I_{yy} the pitch moment of inertia, α the angle of attack and A_W and C_W the axial and normal specific acceleration coordinates in wind axes respectively. Note that the point mass kinematics describe the aircraft's position, velocity magnitude and gross attitude over time, while the rigid body rotational dynamics describes the attitude of the body axis system with respect to the wind axis system (through the angle of attack) as well as how the torques on the aircraft affect this relative attitude. It must be highlighted that the particular form of the equations of motion presented above is in fact readily available in the literature (Etkin, 1972), albeit not appropriately rearranged. However, presenting this particular form within the context of the proposed manoeuvre autopilot architecture and with the appropriate rearrangements will be seen to provide a novel perspective on the form that explicitly highlights the manoeuvre autopilot design concepts. Expanding now the specific acceleration terms with a commonly used pre-stall flight aircraft specific force and moment model yields,

$$A_W = \left(T\cos\alpha - D\right)/m \tag{7}$$

$$C_W = -\left(T\sin\alpha + L\right)/m \tag{8}$$

with,

$$\dot{T} = -T/\tau_T + T_C/\tau_T \tag{9}$$

$$L = qSC_L \tag{10}$$

$$D = qSC_D \tag{11}$$

$$M = qSC_m \tag{12}$$

where m is the aircraft's mass, τ_T the thrust time constant, S the area of the wing, C_L, C_D and C_m the lift, drag and pitching moment coefficients respectively and,

$$q = \rho \bar{V}^2 / 2 \tag{13}$$

the dynamic pressure. Expansion of the aerodynamic coefficients for pre-stall flight (Etkin & Reid, 1995) yields,

$$C_L = C_{L_0} + C_{L_\alpha}\alpha + C_{L_Q}\left(\bar{c}/2\bar{V}\right)Q + C_{L_{\delta_E}}\delta_E \tag{14}$$

$$C_D = C_{D_0} + C_L^2/\pi Ae \tag{15}$$

$$C_m = C_{m_0} + C_{m_\alpha}\alpha + C_{m_Q}\left(\bar{c}/2\bar{V}\right)Q + C_{m_{\delta_E}}\delta_E \tag{16}$$

where A is the aspect ratio, e the Oswald efficiency factor and standard non-dimensional stability derivative notation is used. Note that it is assumed in this chapter that the non-dimensional stability derivatives above are independent of both the point mass and rigid body rotational dynamics states. Although in reality the derivatives do change somewhat with the system states, for many UAVs operating under pre-stall flight conditions this change is small. Furthermore, with the intention being to design a feedback based control system to regulate specific acceleration, the adverse effect of the modelling errors will be greatly reduced thus further justifying the assumption.

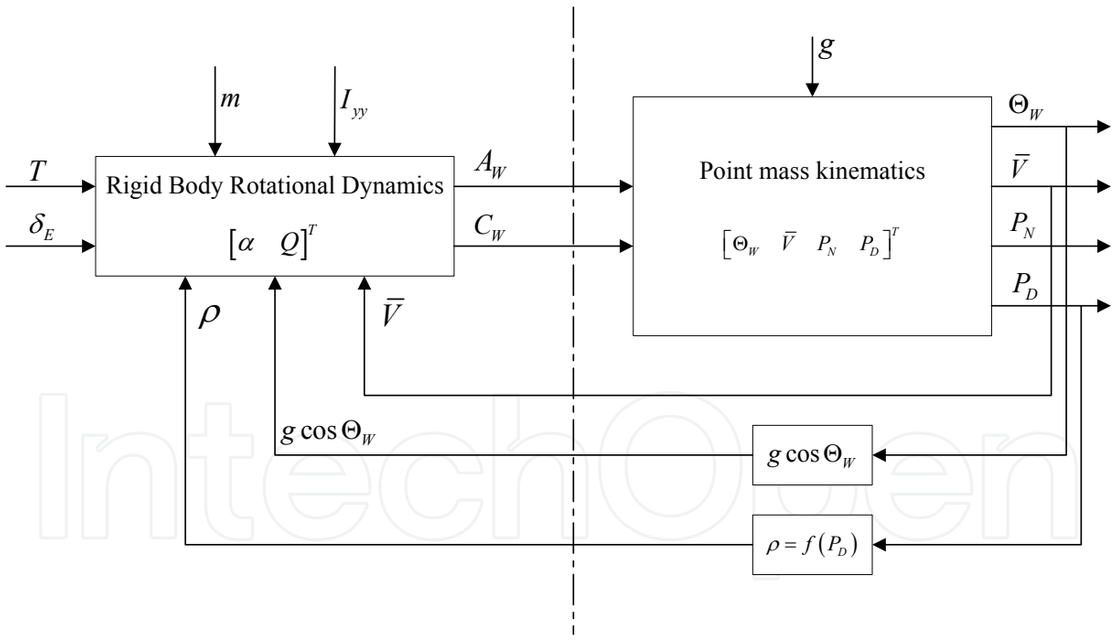


Fig. 1. Split between the rigid body rotational dynamics and the point mass kinematics.

Figure 1 provides a graphical overview of the particular form of the dynamics presented here. The dash-dotted vertical line in the figure highlights a natural split in the aircraft dynamics into the aircraft dependent rigid body rotational dynamics on the left and the aircraft independent point mass kinematics on the right. It is seen that all of the aircraft specific uncertainty resides within the rigid body rotational dynamics, with gravitational acceleration being the only inherent uncertainty in the point mass kinematics. Of course left

unchecked, the aircraft specific uncertainty in the rigid body rotational dynamics would leak into the point mass kinematics via the axial and normal specific acceleration, thus motivating the design of feedback based specific acceleration controllers.

Continuing to analyze Figure 1, the point mass kinematics are seen to link back into the rigid body rotational dynamics via the velocity magnitude, air density (altitude) and flight path angle. If it can be shown that the aforementioned couplings do not strongly influence the rigid body rotational dynamics, then the rigid body rotational dynamics would become completely independent of the point mass kinematics and thus the gross attitude of the aircraft. This in turn would provide the mathematical platform for the design of gross attitude independent specific acceleration controllers.

Investigating the feedback couplings, the velocity magnitude and air density couple into the rigid body rotational dynamics primarily through the dynamic pressure, which is seen in equations (10) through (12) to scale the magnitude of the aerodynamic forces and moments. However, the dynamics of most aircraft are such that the angle of attack and pitch rate dynamics operate on a timescale much faster than that of the velocity magnitude and air density dynamics. Thus, assuming that a timescale separation either exists or can be enforced through feedback control, the dynamic coupling is reduced to a static dependence where the velocity magnitude and air density are treated as parameters in the rigid body rotational dynamics.

The flight path angle is seen to couple only into the angle of attack dynamics, via gravitational acceleration. The flight path angle coupling term in equation (6) represents the tendency of the wind axis system to rotate under the influence of the component of gravitational acceleration normal to the velocity vector. The rotation has the effect of changing the relative attitude of the body and wind axis system as modelled by the angle of attack dynamics. However, the normal specific acceleration (shown in parenthesis next to the gravity term in equation (6)) will typically be commanded by an outer loop guidance controller to cancel the gravity term and then further to steer the aircraft as desired in inertial space. Thus, the effect of the flight path coupling on the angle of attack dynamics is expected to be small. However, to fully negate this coupling, it will be assumed that a dynamic inversion control law can be designed to reject it, the details of which will be discussed in a following section. Note however, that dynamic inversion will only be used to reject the arguably weak flight path angle coupling, with the remainder of the control solution to be purely feedback based.

With the above timescale separation and dynamic inversion assumptions in place, the rigid body rotational dynamics become completely independent of the point mass kinematics and thus provide the mathematical platform for the design of gross attitude independent specific acceleration controllers. With all aircraft specific uncertainty encapsulated within the inner loop specific acceleration controllers and disturbance rejection occurring at an acceleration level, the design is argued to provide a robust solution to the manoeuvre flight control problem. The remainder of this article focuses of the design and simulation of the axial and normal specific acceleration controllers, as well as the associated conditions for their implementation.

4. Decoupling the axial and normal dynamics

Control of the axial and normal specific acceleration is dramatically simplified if the rigid body rotational dynamics can be decoupled into axial and normal dynamics. This

decoupling would allow the axial and normal specific acceleration controllers to be designed independently. To this end, consider equations (7) and (8), and notice that for small angles of attack and typical lift to drag ratios, the equations can be well approximated as follows,

$$A_W \approx (T - D)/m \tag{17}$$

$$C_W \approx -L/m \tag{18}$$

With these simplifying assumptions, the thrust no longer couples into the normal dynamics whose states and controls include the angle of attack, pitch rate and elevator deflection. On the other hand, the normal dynamics states still drive into the axial dynamics through the drag coupling of equation (17). However, through proper use of the bandwidth-limited thrust actuator the drag coupling can be rejected up to some particular frequency. Assuming that effective low frequency disturbance rejection can be achieved up to the open loop bandwidth of the thrust actuator, then only drag disturbance frequencies beyond this remain of concern from a coupling point of view.

Considering now the point mass kinematics, it is clear from equation (2) that the axial specific acceleration drives solely into the velocity magnitude dynamics. Thus uncompensated high frequency drag disturbances will result in velocity magnitude disturbances which in turn will couple back into the rest of the rigid body rotational dynamics both kinematically and through the dynamic pressure. However, the natural integration process of the velocity magnitude dynamics will filter the high frequency part of the drag coupling. Thus, given acceptable deviations in the velocity magnitude, the thrust actuator need only reject enough of the low frequency portion of the drag disturbance for its total effect on the velocity magnitude to be acceptable. By acceptable it is meant that the velocity magnitude perturbations are small enough to result in a negligible coupling back into the rigid body rotational dynamics.

To obtain a mathematical hold on the above arguments, consider the closed loop transfer function from the normalized drag input to the axial specific acceleration output,

$$S_D(s) \equiv \frac{A_W(s)}{D(s)/m} \tag{19}$$

Through proper control system design, the gain of the sensitivity transfer function above can be kept below a certain threshold within the controller bandwidth. The bandwidth of the axial specific acceleration controller will however typically be limited to that of the thrust actuator for saturation reasons. For frequencies above the controller bandwidth, the sensitivity transfer function will display some form of transient and then settle to unity gain. Considering the velocity magnitude dynamics of equation (2), the total transfer function of the normalized drag input to velocity magnitude is then,

$$\frac{\bar{V}(s)}{D(s)/m} = \frac{S_D(s)}{s} \tag{20}$$

Note that the integrator introduced by the natural velocity dynamics will result in diminishing high frequency gains. Equation (20) can be used to determine whether drag

perturbations will result in acceptable velocity magnitude perturbations. Conversely, given the expected drag perturbation spectrum and the acceptable level of velocity magnitude perturbations, the specifications of the sensitivity transfer function can be determined. To ease the process of determining acceptable levels of velocity magnitude perturbations and expected levels of drag perturbations, it is convenient to write these both in terms of normal specific acceleration. The return disturbance in normal specific acceleration due to a normal specific acceleration perturbation can then be used to specify acceptable coupling levels. Relating first normalized drag to normal specific acceleration, use of equation (18) provides the following result,

$$\frac{D/m}{C_W} = -\frac{1}{R_{LD}} \tag{21}$$

where use has been made of the fact that lift is related to drag through the lift to drag ratio R_{LD}. Then, equation (18) can be used to capture the dominant relationship between velocity perturbations and the resulting normal specific acceleration perturbations. Partially differentiating equation (18) with respect to the velocity magnitude yields the desired result,

$$\frac{\partial C_W}{\partial \bar{V}} = \frac{\partial}{\partial \bar{V}} \frac{-qSC_L}{m} \approx \frac{-\rho \bar{V} SC_L}{m} = 2\frac{C_W}{\bar{V}} \tag{22}$$

Combining equations (20) to (22) yields the return disturbance sensitivity function,

$$\begin{aligned} S_{C_W}(s) &\equiv \frac{\partial C_W}{\partial \bar{V}} \cdot \frac{V(s)}{D(s)/m} \cdot \frac{D/m}{C_W} \\ &= \left(-2\frac{C_W}{\bar{V}R_{LD}} \frac{1}{s} \right) S_D(s) \end{aligned} \tag{23}$$

Given an acceptable return disturbance level, the specifications of the sensitivity function of equation (19) can be determined for a particular flight condition. With the velocity magnitude and lift to drag ratio forming part of the denominator of equation (23), the resulting constraints on the sensitivity function are mild for low operating values of normal specific acceleration. Only during very high acceleration manoeuvres, does the sensitivity specification become more difficult to practically realize. This is illustrated through an example calculation at the end of section 5.

Given the above arguments, the drag coupling into the axial specific acceleration dynamics can be ignored if the associated sensitivity function constraint is adhered to when designing the axial specific acceleration controller. With the coupling of the drag term ignored, the axial dynamics become independent of the normal dynamics allowing the controllers to be designed separately. Furthermore, note that the axial dynamics also become independent of the velocity magnitude and the air density. Thus, unlike the normal specific acceleration controller, there is no need for the axial specific acceleration controller to operate on a timescale much faster than these variables. This greatly improves the practical viability of designing an axial specific acceleration control system since most thrust actuators are significantly bandwidth limited. The axial and normal dynamics can thus be decoupled as follows,

Axial Dynamics:

$$\dot{T} = \left[-1/\tau_T\right]T + \left[1/\tau_T\right]T_C \tag{24}$$

$$A_W = \left[1/m\right]T + \left[-D/m\right] \tag{25}$$

Normal Dynamics:

$$\begin{bmatrix}\dot{\alpha}\\ \dot{Q}\end{bmatrix} = \begin{bmatrix}-\frac{L_\alpha}{m\bar{V}} & 1-\frac{L_Q}{m\bar{V}}\\ \frac{M_\alpha}{I_{yy}} & \frac{M_Q}{I_{yy}}\end{bmatrix}\begin{bmatrix}\alpha\\ Q\end{bmatrix} + \begin{bmatrix}-\frac{L_{\delta_E}}{m\bar{V}}\\ \frac{M_{\delta_E}}{I_{yy}}\end{bmatrix}\delta_E + \begin{bmatrix}\frac{g\cos\Theta_W}{\bar{V}} - \frac{L_0}{m\bar{V}}\\ \frac{M_0}{I_{yy}}\end{bmatrix} \tag{26}$$

$$C_W = \begin{bmatrix}-\frac{L_\alpha}{m} & -\frac{L_Q}{m}\end{bmatrix}\begin{bmatrix}\alpha\\ Q\end{bmatrix} + \begin{bmatrix}-\frac{L_{\delta_E}}{m}\end{bmatrix}\delta_E + \begin{bmatrix}-\frac{L_0}{m}\end{bmatrix} \tag{27}$$

where dimensional stability and control derivative notation has been used to remove clutter. Finally, notice that the normal dynamics are simply the classical short period mode approximation (Etkin & Reid, 1995) but have been shown here to be valid for all point mass kinematics states (i.e. all gross attitudes) with the flight path angle coupling term acting as a disturbance input. Intuitively this makes sense since the physical phenomena that manifest themselves into what is classically referred to as the short period mode are not dependent on the gross attitude of the aircraft. Whether an aircraft is flying straight and level, inverted or climbing steeply, its short period motion remains unchanged.

5. Axial specific acceleration controller

In this section a controller capable of regulating the axial specific acceleration is designed. Attention will also be given to the closed loop sensitivity function constraint of equation (23) for a specific return disturbance level. With reference to the axial dynamics of equations (24) and (25) define the following Proportional-Integrator (PI) control law with enough degrees of freedom to allow for arbitrary closed loop pole placement,

$$T_c = -K_A A_W - K_E E_A \tag{28}$$

$$\dot{E}_A = A_W - A_{W_R} \tag{29}$$

where A_{W_R} is the reference axial specific acceleration command. The integrator in the controller is essential for robustness towards uncertain steady state drag and thrust actuator offsets. It is straightforward to show that given the desired closed loop characteristic equation,

$$\alpha_c(s) = s^2 + \alpha_1 s + \alpha_0 \tag{30}$$

the feedback gains that will fix the closed loop poles are,

$$K_A = m\left(\tau_T\alpha_1 - 1\right) \tag{31}$$

$$K_E = m\tau_T\alpha_0 \tag{32}$$

These simple, closed form solution gains will ensure an invariant closed loop axial specific acceleration dynamic response as desired. The controller design freedom is reduced to that of selecting appropriate closed loop poles bearing in mind factors such as actuator saturation and the sensitivity function constraint of the previous section. Investigation of the closed loop sensitivity function for this particular control law yields the following result,

$$S_D(s) = -\frac{s}{\tau_T\alpha_0}\left(\frac{\tau_T s+1}{1}\frac{\alpha_0}{s^2+\alpha_1 s+\alpha_0}\right) \tag{33}$$

For actuator saturation reasons the closed loop axial dynamics bandwidth is typically limited to being close to that of the open loop thrust actuator and thus for reasonable closed loop damping ratios the second order term in parenthesis above can be well approximated by a first order model to simplify the sensitivity function as follows,

$$S_D(s) \approx -\frac{s}{\tau_T\alpha_0}\frac{1}{\tau_A s+1} \tag{34}$$

Here, $\tau_A = 1/(\tau_T\alpha_0)$ is the approximating time constant calculated to match the high frequency sensitivity function asymptotes. Substituting equation (34) into equation (23) yields the return disturbance transfer function,

$$S_{C_W}(s) = 2\frac{C_W}{\bar{V}R_{LD}\tau_T\alpha_0}\frac{1}{\tau_A s+1} \tag{35}$$

Given the maximum allowable gain of the return disturbance transfer function γ, a lower bound constraint on the natural frequency (ω_n) of the closed loop axial control system is calculated by satisfying the inequality

$$\frac{\omega_n}{\omega_T} \geq \sqrt{\left[\frac{2C_W\tau_T}{\bar{V}R_{LD}\gamma}\right]_{\max}} \tag{36}$$

where, $\omega_T = 1/\tau_T$ is the open loop bandwidth of the thrust actuator and the subscript max denotes the maximum value of the term in parenthesis. The following example illustrates the practical feasibility of adhering to the sensitivity function constraint. Consider a UAV that is to fly with a minimum velocity of 20 m/s, with a maximum normal specific acceleration of 4 g and a minimum lift to drag ratio of 10. Then, for more than 20 dB of return disturbance rejection, the natural frequency of the closed loop system should have the following relationship to the open loop thrust bandwidth,

$$\omega_n/\omega_T \geq 2\sqrt{\tau_T} \tag{37}$$

For this specific example, thrust actuators with a bandwidth of below 4 rad/s (time constant of greater than 0.25 s) will require that the closed loop natural frequency is greater than that of the thrust actuator. Despite the fairly extreme nature of this example (low velocity magnitude, high acceleration and low lift to drag ratio), thrust time constants on the order

of 0.25 s are still practically feasible for UAVs. The deduction is thus that the axial specific acceleration controller will be practically applicable to most UAVs.

6. Normal specific acceleration controller

This section presents the design and associated analysis of a closed form normal specific acceleration controller that yields an invariant dynamic response for all point mass kinematics states. The design is based on the linear normal dynamics of equations (26) and (27) with the velocity magnitude and air density considered parameters and the flight path angle coupling rejected using dynamic inversion. To consider the velocity magnitude and air density as parameters requires a timescale separation to exist between these two quantities and the normal dynamics. Therefore, it is important to investigate any upper limits on the allowable bandwidth of the normal dynamics as this will in turn clamp the upper bandwidth of the velocity magnitude and the air density (altitude) dynamics. Furthermore, it is important to investigate the eligibility of the normal dynamics for effective dynamic inversion of the flight path angle coupling term. Thus, before continuing with the normal specific acceleration controller design, the natural normal dynamics are analyzed in detail.

6.1 Natural normal specific acceleration dynamics

Consider the dynamics from the elevator control input to the normal specific acceleration output. The direct feed-through term in the normal specific acceleration output implies that the associated transfer function has as many zeros as it does poles. The approximate characteristic equation for the poles is easily be shown to be,

$$p(s) = s^2 + \left(\frac{L_\alpha}{m\bar{V}} - \frac{M_Q}{I_{yy}} \right) s - \left(\frac{L_\alpha}{m\bar{V}} \frac{M_Q}{I_{yy}} + \frac{M_\alpha}{I_{yy}} \right) \tag{38}$$

where use has been made of the commonly used simplifying assumption (Etkin & Reid, 1995),

$$\left| L_Q / m\bar{V} \right| \ll 1 \tag{39}$$

Considering equation (38) it is important to note that the normal dynamics poles are not influenced by the lift due to pitch rate or elevator deflection. The importance of this will be made clear later on in this section. The zeros from the elevator input to the normal specific acceleration output can be shown, after some manipulation, to be well approximated by the roots of the characteristic equation,

$$s^2 - L_Q \left(l_T - l_D \right) / I_{yy}\, s - L_\alpha \left(l_T - l_N \right) / I_{yy} = 0 \tag{40}$$

with the following characteristic lengths defined,

$$l_N \equiv -M_\alpha / L_\alpha \tag{41}$$

$$l_T \equiv -M_{\delta_E} / L_{\delta_E} \tag{42}$$

$$l_D \equiv -M_Q / L_Q \tag{43}$$

where, l_N is the length to the neutral point, l_T is the effective length to the tail-plane and l_D is the effective damping arm length. Note that only the simplifying assumption of equation (39) has been used in obtaining the novel characteristic equation for the zeros above. Completing the square to find the roots of equation (40) gives,

$$\left[s - L_Q \left(l_T - l_D \right) / 2I_{yy} \right]^2 = \left[L_Q \left(l_T - l_D \right) / 2I_{yy} \right]^2 + L_\alpha \left(l_T - l_N \right) / I_{yy} \tag{44}$$

For most aircraft the effective length to the tail-plane and effective damping arm lengths are very similar. This is because most of the damping arises from the tail-plane which is also typically home to the elevator control surface. Thus the moment arm lengths for pitch rate and elevator deflection induced forces are very similar. As a result, the first term on the right hand side of equation (44) is most often negligibly small and to a good approximation, the zeros from elevator to normal specific acceleration are,

$$z_{1,2} \approx L_Q \left(l_T - l_D \right) / 2I_{yy} \pm \sqrt{L_\alpha \left(l_T - l_N \right) / I_{yy}} \tag{45}$$

Analysis of equation (45) reveals that the only significant effect of the lift due to pitch rate derivative on the zeros is that of producing an offset along the real axis. As previously argued, the effective tail-plane and damping arm lengths are typically very similar and as a result, even this effect is usually small. Thus, it can be seen that to a good approximation, the lift due to pitch rate plays no role in determining the elevator to normal specific acceleration dynamics.

On the other hand, the effective length to the tail-plane and the length to the neutral point typically differ significantly. With this difference scaled by the lift due to angle of attack (which is usually far greater than the lift due to pitch rate) it can be seen that the second term in equation (45) will dominate the first in determining the zero positions. Thus although the lift due to elevator deflection played no role in determining the system poles, it plays a large role in deter-mining the zeros. Knowing the position of the zeros is important from a controller design point of view because not only do they affect the dynamic response of the system but they also impose controller independent limitations on the system's practically achievable dynamic response. These limitations are mathematically described by Bode's sensitivity and complementary sensitivity integrals as discussed in (Freudenberg & Looze, 1985); (Goodwin et al., 2001).

Expanding on the above point, it is noted that for most aircraft the effective length to the tail-plane is far greater than the length to the neutral point and so the zeros are real and of opposite sign. The result, as intuitively expected, is that the dynamics from the elevator to normal specific acceleration are NMP since a Right Half Plane (RHP) zero exists. A RHP zero places severe, controller independent restrictions on the practically attainable upper bandwidth of the closed loop normal specific acceleration dynamics. Furthermore, designing a dynamic inversion control law in a system with NMP dynamics, particularly when the NMP nature of the system is weak, tends to lead to an impractical solution with internal dynamics that may or may not be stable (Hauser et al., 1992); (Hough, 2007).

Since this NMP dynamics case is by far the most common for aircraft, the limits imposed by it shall be investigated further in the following subsection. The goal of the investigation is to seek

a set of conditions under which the effects of a RHP zero become negligible, equivalently allowing the NMP nature of a system to be ignored. With these conditions identified and satisfied, the design of the normal specific acceleration controller can continue based on a set of simplified dynamics that do not capture the NMP nature of the system.

6.2 Analysis of the NMP dynamics case

Ignoring the typically negligible real axis offset term in equation (45), the transfer function from the elevator to normal specific acceleration is of the form,

$$G(s) = k\frac{\omega_n^2}{s^2 + 2\zeta\omega_n s + \omega_n^2}\frac{z_0 - s}{z_0} \tag{46}$$

where z_0 is the RHP zero position. Note that the effect of the left half plane zero has been neglected because it is most often largely negated through pole-zero cancellation by un-modelled dynamics such as those introduced through servo lag. The transfer function of equation (46) can be written as follows,

$$G(s) = G_n(s) - G_n(s)s/z_0 \tag{47}$$

where,

$$G_n(s) = k\frac{\omega_n^2}{s^2 + 2\zeta\omega_n s + \omega_n^2} \tag{48}$$

is a nominal second order system with no zeros. Equation (48) makes it clear that as the position of the zero tends towards infinity, so the total system transfer function converges towards $G_n(s)$. The purpose of the analysis to follow is to investigate more precisely, the conditions under which $G(s)$ can be well approximated by $G_n(s)$. To this end, a time response analysis method is employed. Consider the Laplace transform of the system's step response,

$$Y(s) = G_n(s)/s - G_n(s)/z_0 \tag{49}$$

Equation (49) makes it clear that the total step response is the nominal system step response less the impulse response of the system scaled by the inverse of the RHP zero frequency. Since the nominal response gradient is always zero at the time of the step, the system must exhibit undershoot. The level of undershoot will depend of the damping, speed of response of the system and the zero frequency. If the level of undershoot is small relative to unity then it is equivalent to saying that the second term of equation (47) has a negligible effect. Thus, by investigating the undershoot further, conditions can be developed under which the total system response is well approximated by the nominal system response.

A closed form solution for the exact level of undershoot experienced in response to a step command for a system of the form presented in equation (46) is provided below,

$$y_{\min} = k\left[1 - \left(\sin\theta/\sin\phi\right)e^{-(\theta-\phi)/\tan\theta}\right] \tag{50}$$

where,

$$\theta = \cos^{-1}(\zeta) \tag{51}$$

$$\phi = \tan^{-1}\left(\sqrt{1-\zeta^2}\,/\,(\zeta + r)\right) \tag{52}$$

$$r = \omega_n / z_0 \tag{53}$$

Derivation of this novel result involves inverse Laplace transforming equation (49) and finding the time response minima through calculus. The above equations make it clear that the undershoot is only a function of the ratio between the system's natural frequency and the zero frequency (r) and the system's damping ratio (ζ). Figure 2 below provides a plot of the maximum percentage undershoot as a function of r^{-1} for various damping ratios.

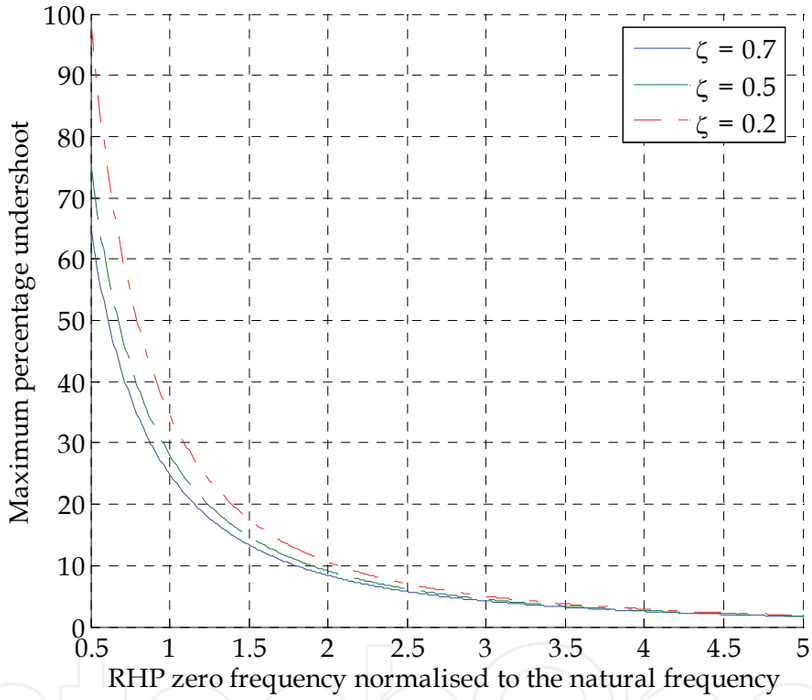


Fig. 2. Maximum undershoot of a 2nd order system as a function of normalized RHP zero frequency for various damping ratios.

It is clear from Figure 2 that for low percentage undershoots, the damping ratio has little influence. Thus, the primary factor determining the level of undershoot is the ratio of the system's natural frequency to that of the zero frequency. Furthermore, it is clear that for less than 5% maximum undershoot, the natural frequency should be at least three times lower than that of the zero. With only 5% undershoot the response of the total system will be well approximated by the response of the nominal system with no zero. Thus by making use of the maximum undershoot as a measure of the NMP nature of a system the following novel frequency domain design rule is developed,

$$\omega_n < z_0/3 \tag{54}$$

for the NMP nature of the system to be considered negligible. This rule implies that the system poles must lie within a circle of radius $z_0/3$ in the s-plane. Thus, an upper bound is placed on the natural frequency of the system if its NMP nature is to be ignored.

6.3 Frequency bounds on the normal specific acceleration controller

Given the results of the previous two subsections, the upper bound on the natural frequency of the normal specific acceleration controller becomes,

$$\omega_n < \left| \sqrt{L_\alpha \left(l_T - l_N \right) / I_{yy}} \right| / 3 \tag{55}$$

where the typically negligible offset in the zero positions in equation (45) has been ignored. Adhering to this upper bound will allow the NMP nature of the system to be ignored and will thus ensure both practically feasible dynamic inversion of the flight path angle coupling and no large sensitivity function peaks (Goodwin et al., 2001) in the closed loop system. Note that given the physical meaning of the characteristic lengths defined in equations (41) through (43), the approximate zero positions and thus upper frequency bound can easily be determined by hand for a specific aircraft.

It is important to note that the upper bound applies to both the open loop and closed loop normal specific acceleration dynamics. If the open loop poles violate the condition of equation (55) then moving them through control application to within the acceptable frequency region will require taking into account the effect of the system zeros. Thus, for an aircraft to be eligible for the normal specific acceleration controller of the next subsection, its open loop normal dynamics poles must at least satisfy the bound of equation (55). If they do not then an aircraft specific normal specific acceleration controller would have to be designed. However, most aircraft tend to satisfy this bound in the open loop because open loop poles outside the frequency bound of equation (55) would yield an aircraft with poor natural flying qualities i.e. the aircraft would be too statically stable and display significant undershoot and lag when performing elevator based manoeuvres. Interestingly, the frequency bound can thus also be utilized as a design rule for determining the most forward centre of mass position of an aircraft for good handling qualities.

In term of lower bounds, the normal dynamics must be timescale separated from the velocity magnitude and air density (altitude) dynamics. Of these two signals, the velocity magnitude typically has the highest bandwidth and is thus considered the limiting factor. Given the desired velocity magnitude bandwidth (where it is assumed here that the given bandwidth is achievable with the available axial actuator), then as a practical design rule the normal dynamics bandwidth should be at least five times greater than this for sufficient timescale separation. Note that unlike in the upper bound case, only the closed loop poles need satisfy the lower bound constraint. However, if the open loop poles are particularly slow, then it will require a large amount of control effort to meet the lower bound constraint in the closed loop. This may result in actuator saturation and thus a practically infeasible controller. However, for typical aircraft parameters the open loop poles tend to already satisfy the timescale separation lower bound.

With the timescale separation lower bound and the NMP zero upper bound, the natural frequency of the normal specific acceleration controller is constrained to lying within a circular band in the s-plane as shown in Figure 3 (poles would obviously not be selected in the RHP for stability reasons). The width of the circular band in Figure 3 is an indication of

the eligibility of a particular airframe for the application of the normal specific acceleration controller to be designed in the following subsection.
For most aircraft this band is acceptably wide and the control system to be presented can be directly applied. For less conventional aircraft, the band can become very narrow and the two constraint boundaries may even cross. In this case, the generic control system to be presented cannot be directly applied. One solution to this problem is to design an aircraft specific normal specific acceleration controller. However, this solution is typically not desirable since the closeness of the bounds suggests that the desired performance of the particular airframe will not easily be achieved practically. Instead, redesign of the airframe and/or reconsideration of the outer loop performance bandwidths will constitute a more practical solution.

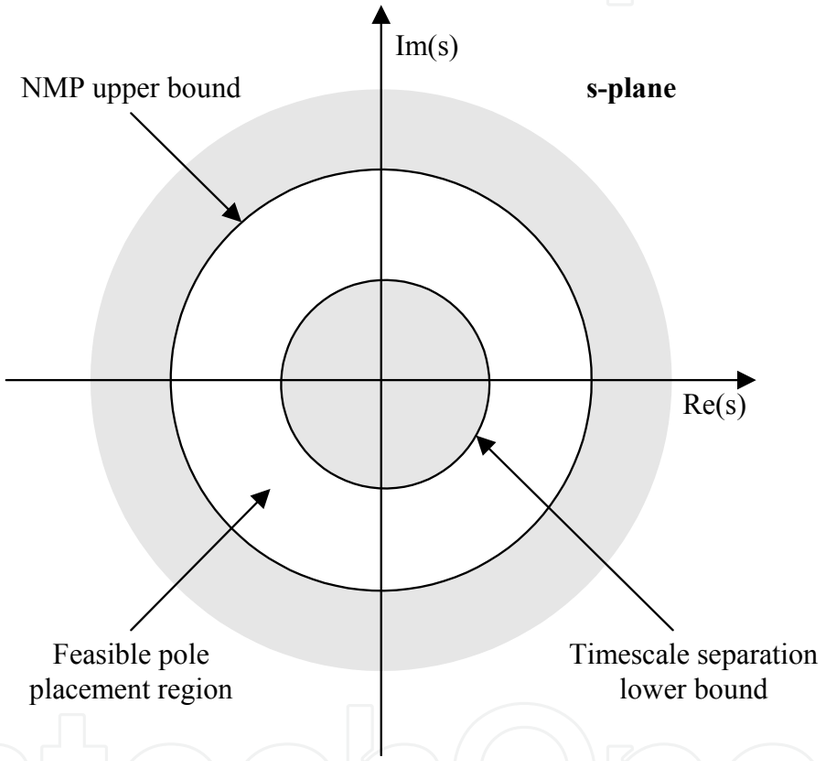


Fig. 3. NMP upper bound and timescale separation lower bound outlining feasible pole placement region.

6.4 Normal specific acceleration controller design

Assuming that the frequency bounds of the previous section are met, the design of a practically feasible normal specific acceleration controller can proceed based on the following reduced normal dynamics,

$$\begin{bmatrix} \dot{\alpha} \\ \dot{Q} \end{bmatrix} = \begin{bmatrix} -\frac{L_\alpha}{m\bar{V}} & 1 \\ \frac{M_\alpha}{I_{yy}} & \frac{M_Q}{I_{yy}} \end{bmatrix} \begin{bmatrix} \alpha \\ Q \end{bmatrix} + \begin{bmatrix} 0 \\ \frac{M_{\delta_E}}{I_{yy}} \end{bmatrix} \delta_E + \begin{bmatrix} \frac{g\cos\Theta_W}{\bar{V}} - \frac{L_0}{m\bar{V}} \\ \frac{M_0}{I_{yy}} \end{bmatrix} \tag{56}$$

$$C_W = \begin{bmatrix} -\frac{L_\alpha}{m} & 0 \end{bmatrix} \begin{bmatrix} \alpha \\ Q \end{bmatrix} + [0]\delta_E + \begin{bmatrix} -\frac{L_0}{m} \end{bmatrix} \tag{57}$$

The simplifications in the dynamics above arise from the analysis of subsection 6.1 where it was shown that to a good approximation, the lift due to pitch rate and elevator deflection only play a role in determining the zeros from elevator to normal specific acceleration. Under the assumption that the upper bound of equation (55) is satisfied, the zeros effectively move to infinity and correspondingly these two terms become zero. Thus, the simplified normal dynamics above will yield identical approximated poles to those of equation (38), but will display no finite zeros from elevator to normal specific acceleration.
To dynamically invert the effect of the flight path angle coupling on the normal specific acceleration dynamics requires differentiating the output of interest until the control input appears in the same equation. The control can then be used to directly cancel the undesirable terms. Differentiating the normal specific acceleration output of equation (57) once with respect to time yields,

$$\dot{C}_W = \begin{bmatrix} -\frac{L_\alpha}{m\bar{V}} \end{bmatrix} C_W + \begin{bmatrix} -\frac{L_\alpha}{m} \end{bmatrix} Q + \begin{bmatrix} -\frac{L_\alpha g \cos\Theta_W}{m\bar{V}} \end{bmatrix} \tag{58}$$

where the angle of attack dynamics of equation (6) have been used in the result above. Differentiating the normal specific acceleration a second time gives,

$$\begin{aligned} \ddot{C}_W = & \left[\frac{M_Q}{I_{yy}} - \frac{L_\alpha}{m\bar{V}} \right] \dot{C}_W + \left[\frac{M_\alpha}{I_{yy}} + \frac{L_\alpha M_Q}{m\bar{V} I_{yy}} \right] C_W \\ & + \left[-\frac{L_\alpha M_{\delta_E}}{m I_{yy}} \right] \delta_E + \left[\frac{L_0 M_\alpha}{m I_{yy}} - \frac{L_\alpha M_0}{m I_{yy}} \right] + \left[\frac{L_\alpha g}{m\bar{V}} \left(\frac{M_Q}{I_{yy}} \cos\Theta_W + \dot{\Theta}_W \sin\Theta_W \right) \right] \end{aligned} \tag{59}$$

where use has been made of equations (56) to (58) in obtaining the result above. The elevator control input could now be used to cancel the effect of the flight path angle coupling terms on the normal specific acceleration dynamics. However, the output feedback control law to be implemented will make use of pitch rate feedback. Upon analysis of equation (6), it is clear that pitch rate feedback will reintroduce flight path angle coupling terms into the normal specific acceleration dynamics. Thus, the feedback control law is first defined and substituted into the dynamics, and then the dynamic inversion is carried out. A PI control law with enough degrees of freedom to place the closed loop poles arbitrarily and allow for dynamic inversion (through $\delta_{E_{DI}}$) is defined below,

$$\delta_E = -K_Q Q - K_C C_W - K_E E_C + \delta_{E_{DI}} \tag{60}$$

$$\dot{E}_C = C_W - C_{W_R} \tag{61}$$

with C_{W_R} the reference normal specific acceleration command. The integral action of the control law is introduced to ensure that the normal specific acceleration is robustly tracked with zero steady state error. Offset disturbance terms such as those due to static lift and pitching moment can thus be ignored in the design to follow. It is best to remove the effect

of terms such as these with integral control since they are not typically known to a high degree of accuracy and thus cannot practically be inverted along with the flight path angle coupling. Upon substitution of the control law above into the normal specific acceleration dynamics of equation (59), the closed loop normal dynamics become,

$$\begin{aligned}\ddot{C}_W = &\left[\frac{L_\alpha M_{\delta_E}}{mI_{yy}}K_E\right]E_C + \left[\frac{M_Q}{I_{yy}} - \frac{L_\alpha}{m\bar{V}} - \frac{M_{\delta_E}}{I_{yy}}K_Q\right]\dot{C}_W \\ &+\left[\frac{M_\alpha}{I_{yy}} + \frac{L_\alpha M_Q}{m\bar{V}I_{yy}} + \frac{L_\alpha M_{\delta_E}}{mI_{yy}}K_C - \frac{L_\alpha M_{\delta_E}}{m\bar{V}I_{yy}}K_Q\right]C_W\end{aligned} \tag{62}$$

$$\dot{E}_C = C_W - C_{W_R} \tag{63}$$

when,

$$\delta_{E_{DI}} = \frac{g}{\bar{V}}\left[\left(\frac{M_Q}{M_{\delta_E}} - K_Q\right)\cos\Theta_W + \left(\frac{I_{yy}}{M_{\delta_E}}\dot{\Theta}_W\right)\sin\Theta_W\right] \tag{64}$$

and the static offset terms are ignored. Note that the dynamic inversion part of the control law is still a function of the yet to be determined pitch rate feedback gain. Given the desired closed loop characteristic equation for the normal dynamics,

$$\alpha_c(s) = s^3 + \alpha_2 s^2 + \alpha_1 s + \alpha_0 \tag{65}$$

the closed form solution feedback gains can be calculated by matching characteristic equation coefficients to yield,

$$K_Q = \frac{I_{yy}}{M_{\delta_E}}\left(\alpha_2 + \frac{M_Q}{I_{yy}} - \frac{L_\alpha}{m\bar{V}}\right) \tag{66}$$

$$K_C = -\frac{mI_{yy}}{L_\alpha M_{\delta_E}}\left(\alpha_1 + \frac{M_\alpha}{I_{yy}} - \frac{L_\alpha}{m\bar{V}}\left(\alpha_2 - \frac{L_\alpha}{m\bar{V}}\right)\right) \tag{67}$$

$$K_E = -\frac{mI_{yy}}{L_\alpha M_{\delta_E}}\alpha_0 \tag{68}$$

Substituting the pitch rate feedback gain into equation (64) gives,

$$\delta_{E_{DI}} = \frac{g}{\bar{V}}\frac{I_{yy}}{M_{\delta_E}}\left[\left(\frac{L_\alpha}{m\bar{V}} - \alpha_2\right)\cos\Theta_W - \left(\frac{C_W + g\cos\Theta_W}{\bar{V}}\right)\sin\Theta_W\right] \tag{69}$$

where use has been made of equation (1) to remove the flight path angle derivative. The controller design freedom is reduced to that of placing the three poles that govern the closed loop normal dynamics. The control system will work to keep these poles fixed for all point mass kinematics states and in so doing yield a dynamically invariant normal specific acceleration response at all times.

7. Simulation

To verify the controller designs of the previous subsections, they are applied to an off-the-shelf scale model aerobatic aircraft, the 0.90 size CAP232, used for research purposes at Stellenbosch University. In the simulations and analysis to follow, the aircraft is operated about a nominal velocity magnitude of 30 m/s and a nominal sea level air density of 1.225 kg/m^3. The modelling parameters for the aircraft are listed in the table below and were obtained from (Hough, 2007).

$m = 5.0$ kg	$A = 5.97$	$C_{L_0} = 0.0$	$C_{m_0} = 0.0$
$I_{yy} = 0.36$ kgm^2	$\tau_T = 0.25$ s	$C_{L_\alpha} = 5.1309$	$C_{m_\alpha} = -0.2954$
$c = 0.30$ m	$e = 0.85$	$C_{L_Q} = 7.7330$	$C_{m_Q} = -10.281$
$S = 0.50$ m^2	$C_{D_0} = 0.02$	$C_{L_{\delta_E}} = 0.7126$	$C_{m_{\delta_E}} = -1.5852$

Table 1. Model parameters for the Stellenbosch University aerobatic UAV

Given that the scenario described in the example at the end of section 5 applies to the aerobatic UAV in question, the closed loop natural frequency of the axial specific acceleration controller should be greater than or equal to the bandwidth of the thrust actuator (4 rad/s) for a return disturbance of -20 dB. Selecting the closed loop poles at {-4±3i}, provides a small buffer for uncertainty in the actuator lag, without overstressing the thrust actuator. Figure 4 provides a Bode plot of the actual and approximated return disturbance transfer functions for this design, i.e. equation (23), with the actual and approximated sensitivity functions of equations (33) and (34) substituted respectively. Also plotted are the actual and approximated sensitivity functions themselves as well as the term in parenthesis in equation (23), i.e. the normalized drag to normalized velocity perturbation transfer function. Figure 4 clearly illustrates the greater than 20 dB of return disturbance rejection obtained over the entire frequency band due to the appropriate selection of the closed loop poles. The figure also shows how the return disturbance rejection is contributed towards by the controller at low frequencies and the natural velocity magnitude dynamics at high frequencies. The plot thus verifies the mathematics of the decoupling analysis done in section 4.

Open loop analysis of the aircraft's normal dynamics reveals the actual and approximated poles (shown as crosses) in Figure 5 and the actual and approximated elevator to normal specific acceleration zeros of {54.7, -46.7} and {54.5, -46.6} respectively. The closeness of the poles in Figure 5 and the similarity of the numerical values above verify equations (38) and (40). The approximate zero positions are used in equation (55) to determine the upper NMP frequency bound shown in Figure 5. The lower timescale separation bound arises as a result of a desired velocity magnitude bandwidth of 1 rad/s (a feasible user selected value). Notice both the large feasible pole placement region and the fact that the open loop poles naturally satisfy the NMP frequency constraint, implying good open loop handling qualities.

The controller of subsection 6.4 is then applied to the system with desired closed loop complex poles selected to have a constant damping ratio of 0.7 as shown in Figure 5. The desired closed loop real pole is selected equal to the real value of the complex poles. The corresponding actual closed loop poles are illustrated in Figure 5. Importantly, the locus of actual closed loop poles is seen to remain similar to that of the desired poles while the upper NMP frequency bound is adhered to. Outside the bound the actual poles are seen to diverge quickly from the desired values.

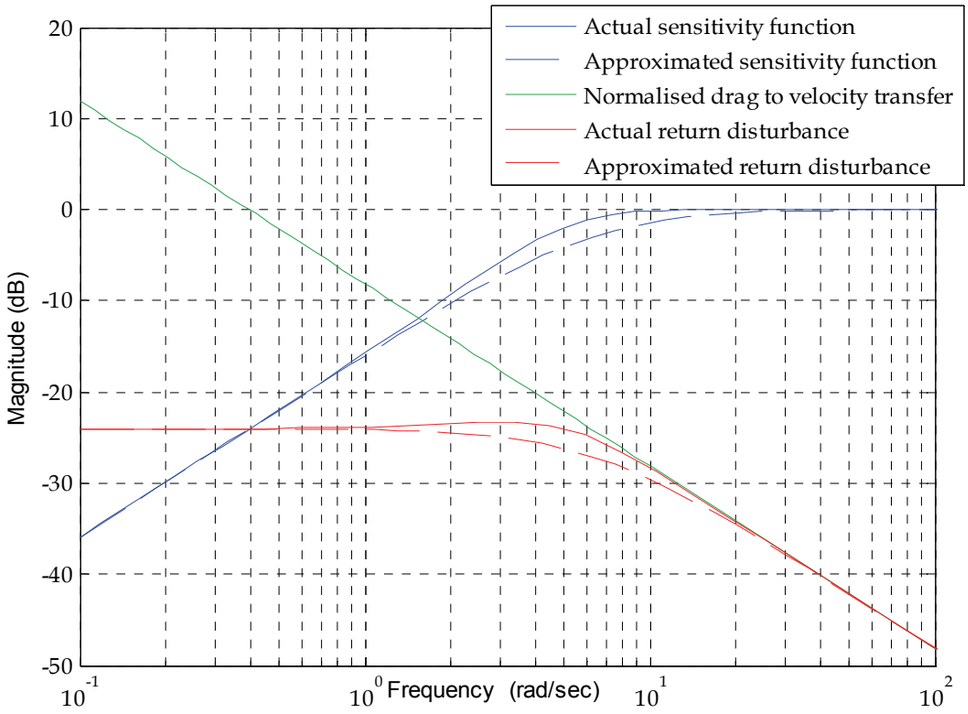


Fig. 4. NMP upper bound and timescale separation lower bound outlining feasible pole placement region.

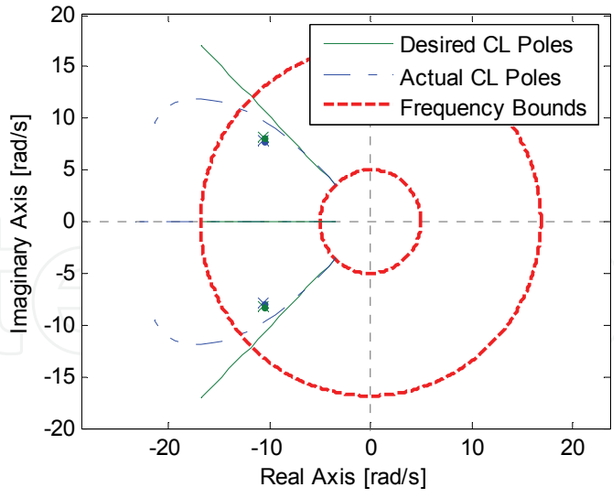


Fig. 5. Actual and approximated open loop (CL) poles, actual and desired closed loop poles and upper and lower frequency bounds.

The controller of subsection 6.4 is then applied to the system with desired closed loop complex poles selected to have a constant damping ratio of 0.7 as shown in Figure 5. The desired closed loop real pole is selected equal to the real value of the complex poles. The corresponding actual closed loop poles are illustrated in Figure 5. Importantly, the locus of

actual closed loop poles is seen to remain similar to that of the desired poles while the upper NMP frequency bound is adhered to. Outside the bound the actual poles are seen to diverge quickly from the desired values.

Figure 6 shows the corresponding feedback gains plotted as a function of the RHP zero position normalized to the desired natural frequency (r^{-1}). The feedback gains are normalized such that their maximum value shown is unity. Again, it is clear from the plot that the feedback gains start to grow very quickly, and consequently start to become impractical, when the RHP zero is less than 3 times the desired natural frequency. The results of Figures 5 and 6 verify the design and analysis of section 6.

Given the analysis above, the desired normal specific acceleration closed loop poles are selected at {-10±8i, -10}. The desired closed loop natural frequency is selected close to that of the open loop system in an attempt to avoid excessive control effort. With the axial and normal specific acceleration controllers designed, a simulation based on the full, nonlinear dynamics of section 3 was set up to test the controllers. Figure 7 provides the simulation results.

The top two plots on the left hand side of the figure show the commanded (solid black line), actual (solid blue line) and expected/desired (dashed red line) axial and normal specific acceleration signals during the simulation. The normal specific acceleration was switched between -1 and -2 g's (negative sign implies 'pull up' acceleration) during the simulation while the axial specific acceleration was set to ensure the velocity magnitude remained within acceptable bounds at all times.

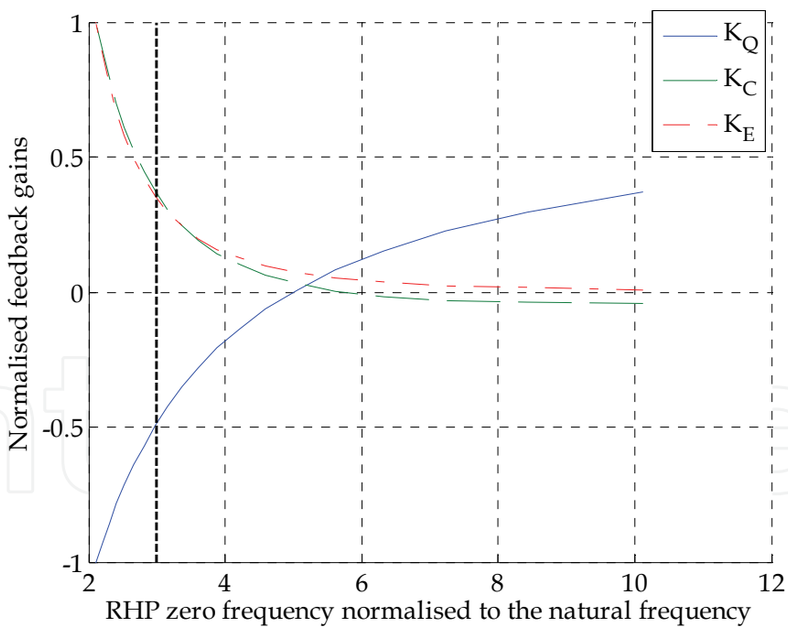


Fig. 6. Normalized controller feedback gains as a function of the RHP zero position normalized to the desired natural frequency.

Importantly, note how the axial and normal specific acceleration remain regulated as expected regardless of the velocity magnitude and flight path angle, the latter of which varies dramatically over the course of the simulation. As desired, the specific acceleration controllers are seen to regulate their respective states independently of the aircraft's velocity

magnitude and gross attitude. The angle of attack, pitch rate, elevator deflection and normalized thrust command are shown on the right hand side of the figure. The angle of attack remains within pre-stall bounds and the control signals are seen to be practically feasible.

Successful practical results of the controllers operating on the aerobatic research aircraft and other research aircraft at Stellenbosch University have recently been obtained. These results will be made available in future publications.

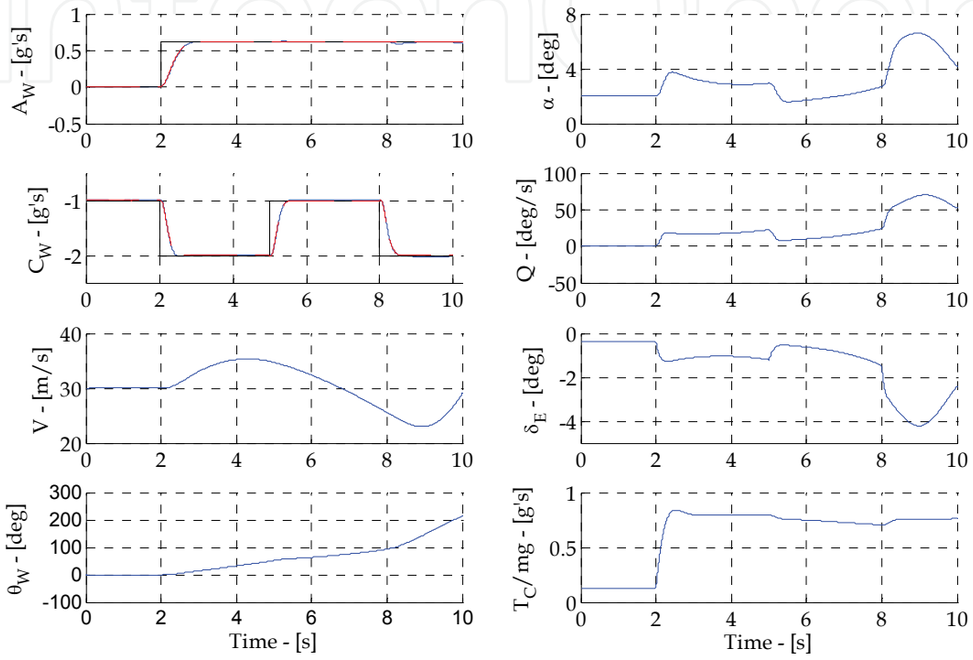


Fig. 7. Simulation results illustrating gross attitude independent regulation of the axial and normal specific acceleration.

8. Conclusion and future work

An acceleration based control strategy for the design of a manoeuvre autopilot capable of guiding an aircraft through the full 3D flight envelope was presented. The core of the strategy involved the design of dynamically invariant, gross attitude independent specific acceleration controllers. Adoption of the control strategy was argued to provide a practically feasible, robust and effective solution to the 3D manoeuvre flight control problem and the non-iterative nature of the controllers provides for a computationally efficient solution.

The analysis and design of the specific acceleration controllers for the case where the aircraft's flight was constrained to the 2D vertical plane was presented in detail. The aircraft dynamics were shown to split into aircraft specific rigid body rotational dynamics and aircraft independent point mass kinematics. With a timescale separation and a dynamic inversion condition in place the rigid body rotational dynamics were shown to be dynamically independent of the point mass kinematics, and so provided a mathematical foundation for the design of the gross attitude independent specific acceleration controllers. Under further mild conditions and a sensitivity function constraint the rigid body rotational

dynamics were shown to be linear and decouple into axial and normal dynamics. The normal dynamics were seen to correspond to the classical Short Period mode approximation dynamics and illustrated the gross attitude independent nature of this mode of motion.
Feedback based, closed form pole placement control solutions were derived to regulate both the axial and normal specific accelerations with invariant dynamic responses. Before commencing with the design of the normal specific acceleration controller, the elevator to normal specific acceleration dynamics were investigated in detail. Analysis of these dynamics yielded a novel approximating equation for the location of the zeros and revealed the typically NMP nature of this system. Based on a time domain analysis a novel upper frequency bound condition was developed to allow the NMP nature of the system to be ignored, thus allowing practically feasible dynamic inversion of the flight path angle coupling.
Analysis and simulation results using example data verified the functionality of the specific acceleration controllers and validated the assumptions upon which their designs were based. Future research will involve extending the detailed control system design to the full 3D flight envelope case based on the autopilot design strategy presented in section 2. Intelligent selection of the closed loop poles will also be the subject of further research. Possibilities include placing the closed loop poles for maximum robustness to parameter uncertainty as well as scheduling the closed loop poles with flight condition to avoid violation of the NMP frequency bound constraint.

9. References

Al-Hiddabi, S.A. & McClamroch, N.H. (2002). Aggressive longitudinal aircraft trajectory tracking using nonlinear control. *Journal of Guidance, Control and Dynamics*, Vol. 25, No. 1, January 2002, pp. 26–32, ISSN 07315090.

Bhattacharya, R.; Balas, G.J.; Kaya, M.A. & Packard, A (2002). Nonlinear receding horizon control of an F-16 aircraft. *Journal of Guidance, Control and Dynamics*, Vol. 25, No. 5, September 2002, pp. 924–931, ISSN 07315090.

Blakelock, J.H. (1991). *Automatic Control of Aircraft and Missiles (2nd Ed.)*, John Wiley and Sons, ISBN 0471506516, New York.

Buffington, J.; Adams, R. & Banda, S. (1993). Robust, nonlinear, high angle-of-attack control design for a super-manoeuvrable vehicle, *Proceedings of the AIAA Guidance, Navigation and Control Conference*, pp. 690–700, Monterey, August 1993.

Bugajski, D.J. & Enns, D.F. (1992). Nonlinear control law with application to high angle-of-attack flight. *Journal of Guidance, Control and Dynamics*, Vol. 15, No. 3, May 1992, pp. 761–767, ISSN 07315090.

Etkin, B. (1972). *Dynamics of Atmospheric Flight*, John Wiley and Sons, ISBN-10 0471246204, New York.

Etkin, B. & Reid, L.D. (1995). *Dynamics of Flight Stability and Control (3rd Ed.),* John Wiley and Sons, ISBN 0471034185, New York.

Freudenberg, J.S. & Looze, D.P. (1985). Right-half plane poles and zeros and design tradeoffs in feedback systems. *IEEE Transactions on Automatic Control*, Vol. 30, No. 6, June 1985, pp. 555-565, ISSN 00189286.

Goodwin, G.C.; Graebe, S.F. & Salgado, M.E. (2001). *Control System Design*, Prentice Hall, ISBN-10 0139586539, Upper Saddle River.

Hauser, J.; Sastry, S. & Meyer, G. (1992). Nonlinear control design for slightly non-minimum phase systems: Application to V/STOL aircraft. *Automatica*, Vol. 28, No. 4, April 1992, pp. 665–679, ISSN 00051098.

Hough, W.J. (2007). *Autonomous Aerobatic Flight of a Fixed Wing Unmanned Aerial Vehicle*, Masters thesis, Stellenbosch University.

Kim, M.J.; Kwon, W.H.; Kim, Y.H. & Song, C. (1997). Autopilot design for bank-to-turn missiles using receding horizon predictive control scheme. *Journal of Guidance, Control and Dynamics*, Vol. 20, No. 6, November 1997, pp. 1248–1254, ISSN 07315090.

Lane, S.H. & Stengel, R.F. (1988). Flight control design using non-linear inverse dynamics. *Automatica*, Vol. 24, No. 4, April 1988, pp. 471–483, ISSN 00051098.

Leith, D.J. & Leithead, W.E. (2000). Survey of gain scheduling analysis & design, *International Journal of Control*, Vol. 73, No. 11, July 2000, pp. 1001-1025, ISSN 00207179.

Miller, R.B. & Pachter, M. (1997). Manoeuvring flight control with actuator constraints. *Journal of Guidance, Control and Dynamics*, Vol. 20, No. 4, July 1997, pp. 729–734, ISSN 07315090.

Pachter, M.; Chandler P.R. & Smith, L. (1998). Manoeuvring flight control. *Journal of Guidance, Control and Dynamics*, Vol. 21, No. 3, May 1998, pp. 368–374, ISSN 07315090.

Peddle, I.K. (2008). *Acceleration Based Manoeuvre Flight Control System for Unmanned Aerial Vehicles*, PhD thesis, Stellenbosch University.

Reiner, J.; Balas, G.J. & Garrard, W.L. (1996). Flight control design using robust dynamic inversion and time-scale separation. *Automatica*, Vol. 32, No. 11, November 1996, pp. 1493–1504, ISSN 00051098.

Slotine, J.E. & Li, W. (1991). *Applied Nonlinear Control*, Prentice Hall, ISBN-10 0130408905, Upper Saddle River.

Snell, S.A.; Enns, D.F. & Garrard, W.L. (1992). Nonlinear inversion flight control for a super-manoeuvrable aircraft. *Journal of Guidance, Control and Dynamics*, Vol. 15, No. 4, July 1992, pp. 976–984, ISSN 07315090.

IntechOpen



Advances in Flight Control Systems

Edited by Dr. Agneta Balint

ISBN 978-953-307-218-0
Hard cover, 296 pages
Publisher InTech
Published online 11, April, 2011
Published in print edition April, 2011

Nonlinear problems in flight control have stimulated cooperation among engineers and scientists from a range of disciplines. Developments in computer technology allowed for numerical solutions of nonlinear control problems, while industrial recognition and applications of nonlinear mathematical models in solving technological problems is increasing. The aim of the book Advances in Flight Control Systems is to bring together reputable researchers from different countries in order to provide a comprehensive coverage of advanced and modern topics in flight control not yet reflected by other books. This product comprises 14 contributions submitted by 38 authors from 11 different countries and areas. It covers most of the currents main streams of flight control researches, ranging from adaptive flight control mechanism, fault tolerant flight control, acceleration based flight control, helicopter flight control, comparison of flight control systems and fundamentals. According to these themes the contributions are grouped in six categories, corresponding to six parts of the book.

How to reference

In order to correctly reference this scholarly work, feel free to copy and paste the following:

Iain K. Peddle and Thomas Jones (2011). Acceleration-based 3D Flight Control for UAVs: Strategy and Longitudinal Design, Advances in Flight Control Systems, Dr. Agneta Balint (Ed.), ISBN: 978-953-307-218-0, InTech, Available from: http://www.intechopen.com/books/advances-in-flight-control-systems/acceleration-based-3d-flight-control-for-uavs-strategy-and-longitudinal-design

INTECH
open science | open minds

InTech Europe
University Campus STeP Ri
Slavka Krautzeka 83/A
51000 Rijeka, Croatia
Phone: +385 (51) 770 447
Fax: +385 (51) 686 166
www.intechopen.com

InTech China
Unit 405, Office Block, Hotel Equatorial Shanghai
No.65, Yan An Road (West), Shanghai, 200040, China
中国上海市延安西路65号上海国际贵都大饭店办公楼405单元
Phone: +86-21-62489820
Fax: +86-21-62489821

© 2011 The Author(s). Licensee IntechOpen. This chapter is distributed under the terms of the Creative Commons Attribution-NonCommercial-ShareAlike-3.0 License, which permits use, distribution and reproduction for non-commercial purposes, provided the original is properly cited and derivative works building on this content are distributed under the same license.

IntechOpen

IntechOpen